Liminana, P.; Garcia-Sanoguera, D.; Quiles-Carrillo, L.; Balart, R.; Montanes, N. (07-2). Development and characterization of environmentally friendly composites from poly(butylene succinate) (PBS) and almond shell flour with different compatibilizers. Composites Part B Engineering. 144:153-162. https://doi.org/10.1016/j.compositesb.2018.02.031

"Development and characterization of environmentally friendly composites from poly(butylene succinate) (PBS) and almond shell flour with different compatibilizers"

P. Limiñana[a], D. Garcia-Sanoguera[a], L. Quiles-Carrillo[a], R. Balart[a], N. Montanes[a]

(a) **Instituto de Tecnología de Materiales (ITM)**
Universitat Politècnica de València (UPV) Plaza Ferrándiz y Carbonell 1, 03801, Alcoy (Alicante), Spain

Corresponding author: L. Quiles-Carrillo (luiquic1@epsa.upv.es)

Abstract

This work reports the enhancement of the properties of poly(butylene succinate) (PBS) composites containing 30 wt% almond shell flour (ASF) by using different compatibilizer families: epoxy, maleic anhydride and acrylic. With regard to the epoxy compatibilizers, epoxidized linseed oil (ELO) and epoxidized soybean oil (ESBO) were used. Two maleic anhydride-derived compatibilizers, namely, maleinized linseed oil (MLO) and dodecenyl succinic anhydride (DDSA) were used. Finally, two acrylic monomers, namely methyl methacrylate (MMA) and acrylic acid (AA) were employed. Uncompatibilized and compatibilized PBS/ASF composites were characterized in terms of their mechanical properties, morphology, thermal behaviour and thermomechanical performance. The obtained results suggest that all three vegetable oil-derived compatibilizers (ELO, ESBO and MLO) give a remarkable increase in ductile properties while poor compatibilization is obtained with the acrylic monomers. These vegetable-oil derived compatibilizers could represents an interesting environmentally friendly solution to compatibilizing polyester-type polymers and their composites with lignocellulosic materials.

Keywords: A-Polymer-matrix composites (PMCs); B-Mechanical properties, B: Thermomechanical; D-Electron microscopy; Compatibilizers.

1. Introduction

Today, a remarkable sensitiveness about the use of environmentally friendly polymers has been detected. Recent trend in the plastic industry focus on reducing petroleum dependency and the corresponding carbon footprint. The worldwide production of plastics, around 300 Mt/year; so that, the plastic industry generates a huge amount of wastes. For this reason, the disintegration potential is a key feature in the development of new materials. Today, it is possible to find a wide range of petroleum-based polyesters that can undergo biodegradation under controlled compost soil conditions. Among these, it is worthy to note the increaseing use of poly(butylene succinate) – (PBS), poly(ε-caprolactone) – (PCL), poly(glycolic acid) – (PGA), poly(butylene succinate-*co*-adipate) – (PBSA), poly(butylene adipate-*co*-terephthalate) – (PBAT)[1]. On the other hand, new developments in the field of renewable and biodegradable polymers are being intensified. These include developments on polysaccharide polymers (cellulose, chitosan, chitin, starch, and so on), protein based polymers (gluten, ovalbumin, soy protein, casein, among others) and bacterial polymers such as poly(3-hydroxybutyrate) – (PHB) or poly(3-hydroxybutyrate-*co*-3-hydroxyvalerate) [2].

Together with the developments on new polymers, an increasing interest on natural fiber reinforced plastics [NFRP) [3, 4] and/or wood plastic composites (WPC) [5] has been observed. The cellulosic reinforcement could positively contribute to high environmental efficiency composite materials and, in addition, upgrade industrial and agroforestry wastes [6]. Many researches have focused on NFRP/WPCs with commodity plastics such as poly(ethylene) (PE) or poly(propylene) (PP), reinforced with vegetable fibers such as date palm [7], kenaf fiber [8], among others. The use of

biopolyesters has broadened the potential of WPCs and NFRP. Thus, some researches on poly(lactic acid) (PLA) with almond shell [9] or nut shell [10] have been reported. Many wastes from the food industry such as nut shell [11], hazelnut shell [12] o coconut [13], could find new uses as reinforcing fillers in high environmentally friendly composite materials.

With regard to almond shell, Spain is the second worldwide producer, just after USA. Almond shell has been successfully used in several biocomposites as reinforcement filler [14-16]. The most important drawback of using cellulosic fillers into polymer matrices is the lack of (or very poor) polymer-particle interactions as typically, polymers are highly hydrophobic, while lignocellulosic fillers are highly hydrophilic [12, 14, 17, 18]. This lack of interactions is responsible for a decrease in mechanical performance, mainly in ductile properties which are highly dependent on cohesion [19]. Therefore, new formulations are being investigated with the main aim of improving the polymer-particle interaction. The use of compatibilizers represents a cost-effective method to improve ductile properties of a composite material by acting as a bridge between the highly hydrophobic matrix and the highly hydrophilic lignocellulosic particles [12].

Among all compostable polyesters, poly(butylene succinate) (PBS) **(Figure 1)** owns a key position as it can be either obtained from petroleum sources or, from renewable resources [20], as both succinic acid and 1,4-butanediol can be bio-derived (*e.g.* BioAmber Inc.). PBS can be fully disintegrated in controlled compost soil [21].

Figure 1

The main uses of PBS include agriculture (padded parts, flanges), packaging industry (disposable cutlery, households, bottles, etc.) [22]. Despite all positive issues of PBS, this is not a widely used polymer due to its high price compared to other conventional plastics. Different composite materials have been developed with PBS matrix with two main objectives. On one hand, to obtain new wood composite materials and on the other hand, to reduce the overall cost of the manufactured material by using a lignocellulosic waste filler. It is worthy to note the use of several natural fibers [23, 24], and natural wastes such as jute fiber [25], hemp fiber [26] pineapple fiber [27]. As above mentioned, compatibilizer agents are needed to provide increased interactions between the polymer matrix and the dispersed lignocellulosic particles.[28]

There are several options to improve this compatibility. Maleinized natural oils, as maleinized linseed oil (MLO) have been successfully used to improve mechanical properties of poly(lactic acid) (PLA) blends with thermoplastic starch (TPS) as reported by Ferri *et al.* On the other hand, Garcia-Garcia et al. reported interesting interactions between MLO and poly(3-hydroxybutyrate) with a clear plasticization and chain extension effect [29, 30]. It is also worthy to note the compatibilizer effect that epoxidized vegetable oils (EVOs) can give to polyester/lignocellulosic composites [2, 12]. Finally, acrylic functionalities have been successfully employed to react with both polymer and particle filler to give interesting compatibilized composites [31].

As PBS is highly expensive and flexible polyester, one interesting solution is to use it as matrix for composites with a low cost lignocellulosic waste such as almond shell flour (ASF). As it is well known, typical interactions in polymer/lignocellulosic composites are poor and contribute to poor mechanical properties [32]. The main aim of this work is the evaluation of the effectiveness of different compatibilizer families:

epoxidized vegetable oils, maleinized compounds and acrylic-acid derived compounds, in terms of mechanical, thermal, thermomechanical and morphological properties of compatibilized PBS/ASF composites.

2. Experimental

2.1. Materials

A poly(butylene succinate) (PBS) commercial grade Bionell 1020MD was supplied by Showa Denko Europe (Munich, Germany). This grade possesses a melt flow index (MFI) of 20 – 34 g/(10 min) and a density of 1.26 g cm^{-3}. Almond shell flour (ASF) was provided in powder form by JESOL Materias Primas (Valencia, Spain). To obtain a homogeneous particle size, the powder was sieved in a vibrating grinder RP09 CISA® (Barcelona, Spain). An average particle size of 150 μm was obtained after sieving.

Compatibilizing of PBS and ASF composites was carried out with different compatibilizer families (see **Figure 2**). The first family of compatibilizers is characterized by the epoxy/oxirane functionality. Two commercial epoxidized vegetable oils, namely epoxidized linseed oil (ELO) and epoxidized soybean oil (ESBO) were supplied by Traquisa S.L. (Barcelona, Spain). The second compatibilizer group is based on maleic anhydride functionality. Two different maleinized compatibilizers were selected. On one hand, a petroleum-derived dodecenyl succinic anhydride (DDSA) supplied by Sigma Aldrich S.A. (Madrid, Spain) and, on the other hand, a renewable sourced maleinized linseed oil (MLO) VEOMER LIN from Vandeputte (Mouscron, Belgium) were used. The last compatibilizer group is based on the acrylic acid functionality. In particular, two petroleum-derive acrylic monomers, namely

methyl methacrylate (MMA) and acrylic acid (AA) were supplied by Sigma Aldrich S.A. (Madrid, Spain).

Figure 2

2.2. Manufacturing of PBS/ASF composites

Poly(butylene succinate) (PBS) and almond shell flour (ASF) were dried at 50 ºC for 24 h. The epoxidized and maleinized vegetable oils (ELO, ESBO y MLO) were heated at 40 ºC for 30 min to decrease viscosity. **Table 1** summarizes the coding and compositions of the developed composites.

Table 1

Initially, a mechanical mixing was carried out manually in a zipper bag for 5 min to achieve basic homogenization. After this, the mixtures were subjected to an extrusion process in a twin-screw co-rotating extruder from Construcciones Mecánicas Dupra S.L. (Alicante, Spain) equipped with a screw diameter of 25 mm and a length to diameter (L/D) ratio of 24. The rotation speed was adjusted to 40 rpm and the temperature profile was set as follows: 120 ºC – 125 ºC – 130 ºC and 130 ºC (from the hopper to the extrusion die). The obtained materials were then pelletized and subsequently dried at 50 ºC for 24 h for further processing by injection molding. The injection molding of standardized samples was carried out in a Meteor 270/75 from Mateu & Solé (Barcelona, Spain) injection machine. The temperature profile was programmed at 110 ºC (hopper), 115 ºC, 120 ºC and 125 ºC (injection nozzle).

2.3. Mechanical characterization

Tensile characterization was carried out in a universal test machine ELIB 50 from S.A.E. Ibertest (Madrid, Spain) as recommended in ISO 527-1:2012. All the tensile tests were conducted using a load cell of 5 kN and a crosshead rate of 10 mm min^{-1}. In addition, Shore D hardness values were obtained in a 676-D durometer from J. Bot Instruments (Barcelona, Spain) following ISO 868:2003. The impact strength was measured using the Charpy method in a 1 J pendulum from Metrotec (San Sebastián, Spain), with standardized notched samples ("V" type with a radius of 0.25 mm) as suggested by ISO 179-1:2010. At least five different samples were tested for each mechanical test and the corresponding values were calculated and averaged. All tests were carried out at room temperature.

2.4. Morphological characterization

The morphology of the fractured samples from impact tests was resolved by field emission scanning electron microscopy in a FESEM microscope ZEISS ULTRA 55 from Oxford Instruments (Abingdon, United Kingdom) working at an accelerating voltage of 2 kV. To avoid electrical charge of samples during observation, all surfaces were covered with a thin Au-Pd alloy in a high vacuum sputter coater EMITECH mod. SC7620 from Quorum Technologies Ltd. (East Sussex, United Kingdom). In addition, samples of PBS/ASF were cryo-fractured by immersion in liquid nitrogen and subsequently broken and observed by FESEM. This allows observing polymer/particle interactions without plastic deformation.

2.5. Thermal characterization

The main thermal transitions were obtained by differential scanning calorimetry (DSC) in a 821 calorimeter from Mettler-Toledo (Schwerzenbach, Switzerland). Samples with an average mass of 5 – 6 mg were subjected to a temperature program in three steps: initially, a heating stage from 30 ^{o}C up to 200 ^{o}C was applied; then, a cooling process down to -50 ^{o}C was scheduled and, finally, a second heating ramp from -50 ^{o}C to 300 ^{o}C was programmed. The heating/cooling rate for all three stages was set to 10 ^{o}C min^{-1}, in nitrogen atmosphere (66 mL min^{-1}). Standard aluminium sealed crucibles with a total volume of 40 mL were used. All DSC ramps were run in triplicate to obtain reliable results. The degree of crystallinity (Xc) was calculated by using the following equation (**Equation 1**):

$$X_C = \left[\frac{\Delta H_m}{\Delta H_m^0 \cdot (1-w)}\right] \cdot 100 \qquad \textbf{Equation 1}$$

Where ΔH_m corresponds to the melt enthalpy. ΔH^0_m (J g^{-1}) stands for the melt enthalpy of a theoretically fully crystalline PBS, with a value of 110.3 J g^{-1} for PBS [33].

Thermal stability at elevated temperatures was followed by thermogravimetric analysis (TGA) in a TGA/SDTA 851 thermobalance from Mettler-Toledo (Schwerzenbach, Switzerland). Samples, with an average weight of 6 mg were placed into standard alumina crucibles with a total volume of 70 mL and were subsequently subjected to a heating program from 30 ^{o}C up to 700 ^{o}C at a constant heating rate of 20 ^{o}C min^{-1} in air atmosphere.

2.6. Thermomechanical characterization

Dynamic mechanical properties of PBS/ASF composites were obtained using dynamic mechanical thermal analysis (DMTA) in an oscillatory rheometer AR-G2 from TA Instruments (New Castle, USA) equipped with a special clamp system for solid samples working in a combination of torsion and shear. Samples sizing 40x10x4 mm^3 were subjected to a temperature sweep from -50 ^oC up to 80 ^oC at a constant heating rate of 2 $^oC\ min^{-1}$ and constant frequency (1 Hz). The maximum strain amplitude (%γ) was set to 0.1%. The storage modulus (G') and the damping factor (tan δ) were collected as a function of increasing temperature.

Dimensional stability was assessed by obtaining the coefficient of linear thermal expansion (CLTE) in a thermomechanical analyser (TMA) mod. Q400 from TA Instruments (New Castle, USA). Samples with dimensions 10x10x4 mm^3 were subjected to a heating ramp from -90 ^oC up to 80 ^oC at a heating rate of 2 $^oC\ min^{-1}$. The applied force was 20 mN.

3. Results and discussion

3.1. Mechanical properties of compatibilized PBS/ASF composites

Figure 3 shows a comparative plot of representative stress-strain curves. Mechanical properties of PBS/ASF compatibilized with different functionalities are summarized in **Table 2.**

Figure 3

Table 2

With regard to tensile properties, it is worthy to note the typical effect of a filler on a polymeric matrix. This is a decrease in both tensile strength and elongation at

break which, in turn, are responsible for an increase in the tensile elastic modulus as it represents the ratio between the applied stress and the elongation in the linear region. Although both parameters are reduced, the elongation is still more sensitive to presence of fillers and this leads to high elastic modulus values. This behaviour is typical of filled polymers in which poor polymer-particle interactions are detected, so that, the overall cohesion is poor. Therefore, the finely dispersed filler particles could act as stress concentrators, leading to lowering both tensile strength and elongation at break. As previously indicated, PBS shows a tensile strength similar to that of PE or PP, at about 31.5 MPa. As it can be seen, the composite with 30 wt% ASF shows a remarkable decrease in tensile strength down to values of 14.8 MPa (which represents a percentage decrease of about 50%). If this decrease is important, the decrease in elongation at break is dramatic as it changes from 215% for neat PBS down to 6.3% for the PBS/ASF uncompatibilized composite. This behaviour gives clear evidences of the poor polymer-particle interactions which are responsible for the dramatic decrease in both tensile strength and elongation at break, due to stress concentration phenomena as a consequence of poor material cohesion. As above mentioned, as the elastic modulus stands for the ratio between the applied stress and the corresponding elongation (in the linear region), it increases thus leading to stiffer materials. Specifically, the tensile modulus of neat PBS, around 417 MPa, is increased up to values of 787.9 MPa in the composite with 30 wt% ASF. Similar findings have been reported by Liu *et al.* in PBS/jute composites which show a dramatic decrease in the elongation at break and tensile strength in composites with 30 wt% jute fiber. In a similar way, the tensile modulus is remarkably increased [34].

Compatibilizers can overcome (or minimize) this drawback. As it can be seen in **Table 2**, all compatibilizers provide increased elongation at break together with a

reduction of the tensile modulus with regard to uncompatibilized PBS/ASF composite. This indicates that the material's cohesion has been improved, thus, the loads can be transferred in a better way between the particle filler and the polymer matrix and this has a positive effect on both mechanical resistant (tensile strength) and ductile (elongation at break) properties as both them are highly sensitive to cohesion. Epoxy-based compatibilizers show a plasticizing effect together with a compatibilizing effect. The tensile strength that both ELO and ESBO provide is close to 13.5 MPa (slightly lower than uncompatibilized PBS/ASF composite). Nevertheless, the elongation at break increases up to values of 14.5% and 13.1% for ELO and ESBO respectively which are remarkably higher compared to uncompatibilized PBS/ASF composite (around 6.3%). Zhao *et al.* reported a remarkable increase in ductile properties when ESBO was added to neat PBS, thus showing the plasticization effect that ESBO could provide [29]. Maleic anhydride-based compatibilizers show interesting results, especially in the case of MLO which gives the highest elongation at break (25.9%) without compromising the tensile strength which remains close to 14 MPa. On the other hand, DDSA also contributes to increased elongation at break (16.9%) and similar tensile strength to uncompatibilized PBS/ASF composite [12, 35, 36]. Conventional compatibilizers contribute to improving the load and stress transfer between the matrix and the particles, in such a way that the increased interaction results in an increase in the modulus. However, compatibilizers derived from vegetable oils provide a reduction of the elastic modulus, and this is related to the intrinsic flexibility of the modified triglyceride molecules. In addition, vegetable oils not only act as compatibilizer agents since, but also lead to PBS chain extension, branching and, potentially, crosslinking, all these processes having somewhat interactions with lignocellulosic particles [37, 38]. It is worthy to note that MLO gives the lowest tensile modulus, of about 534.6 MPa thus

giving clear evidences of the compatibilizing effect of MLO. It is well known that some of the compatibilizers are used as plasticizers. However, due to their particular functionality they also offer the possibility of extending the chain in polyesters, and also some branching and crosslinking. This is due to the high reactivity of the epoxy and maleic anhydride groups with the hydroxyl groups, present both in the terminal groups of the polybutylene succinate (PBS) chains[39, 40]. On the other hand, the compatibilization effect with lignocellulosic residues has also been reported since both functionalities can react simultaneously with the terminal hydroxyl groups of the polyester chains and the hydroxyls present on the surface of the almond shell lignocellulosic particles[9].

With regard to the acrylic-based compatibilizers, both them (MMA and AA) do not give improved properties with similar mechanical properties to those of the uncompatibilized PBS/ASF composite. Probably this is due to the fact that acrylic compatibilizers, typically, copolymers or oligomers, start showing important effects on ductility at higher loadings [41].

Addition of a lignocellulosic filler gives, usually, increased hardness as it can be seen in **Table 2**. Therefore, the Shore D hardness is increased from 60.1 (neat PBS) up to 71.2 for uncompatibilized PBS/ASF composite. Although slight changes in Shore D values can be found, it is difficult to establish a direct relationship with the compatibilizer effect. Nevertheless, the impact strength gives interesting results on the effectiveness of the different compatibilizers. The stress concentration due to poor polymer-particle interactions (and cohesion) is clearly seen by a dramatic decrease in the impact strength values which change from 16.5 kJ m^{-2} for the neat PBS down to 1.8 kJ m^{-2} for the uncompatibilized composite. These dramatic decrease in the impact-

absorbed energy is directly related to the extremely high decrease in elongation at break as described before since the energy absorption mainly occurs during deformation and fracture processes. Although the use of compatibilizers is not enough to recover the impact strength values of the neat PBS, it is true that they contribute to minimize the effects of the poor polymer-particle interactions. Once again, vegetable oil derived compatibilizers, *i.e.* ELO, ESBO and MLO give the best performance in terms of impact-absorbed energy. Functionalized vegetable oils (epoxidized or maleinized) are quite flexible molecules with several epoxy or maleic anhydride groups that can either react with hydroxyl groups in PBS and hydroxyl groups in the lignocellulosic filler as it is shown in **Figure 4**. In fact, both epoxidized and maleinized vegetable oils have been suggested to provide different effects on polyester type polymers and their composites with cellulosic materials. As above mentioned, this improvement is not only related to plasticizing phenomena, but also to various processes such as chain extension, compatibilization, branching, crosslinking, due to the high reactivity of the epoxy and maleic anhydride groups towards hydroxyl groups in both PBD end chains and cellulose particles. This behaviour has been reported by Ferri *at al.* in PLA plasticized with MLO. The only addition of 3.5 wt% MLO led to an increase in the impact-absorbed energy from 30.9 kJ m^{-2} up to more than double (62.9 kJ m^{-2}) [42].

Figure 4

It should be mentioned that the acrylic compatibilizers have more active points per unit gram, so it could be expectable a more intense effect on compatibilization. Nevertheless, both epoxy- and maleic anhydride-derived compatibilizers seem to give

better results. This could be related to the fact that both epoxy and maleic anhydride functionalities are more readily to react towards hydroxyl groups in cellulose. For this reason, both epoxy and maleic anhydride-derived compatibilizers give better results than acrylic-based compatibilizers [43]

3.2. Morphology

Mechanical properties are directly related to the morphology of composites. **Figure 5** shows SEM images of cryo-fractured samples corresponding to PBS/ASF composites with different compatibilizers. **Figure 5b** shows a brittle fracture of the uncompatibilized PBS/ASF composite. In addition, a very poor particle-polymer interaction can be detected. In fact, there is an important gap between the ASF and the surrounding PBS matrix. The typical spotted surface of almond shell can be observed in both isolated particle and in the polymer matrix, therefore indicating easy debonding during fracture. In general, highly hydrophilic cellulosic fillers do not show good compatibility with most of polymer matrices (highly hydrophobic) [44]. A previous surface treatment or the use of a compatibilizer is usually needed to reduce this poor interactions [28].

Figure 5

The effect of all compatibilizers on improving particle-polymer interactions is positive. **Figure 5c** and **Figure 5d** show the SEM images corresponding to ELO- and ESBO-compatibilized composites, respectively. In both cases, the gap between the ASF and the surrounding matrix is lower. In the case of the ELO-compatibilized PBS/ASF composite, this gap is almost undetectable. Similar behaviour can be observed by using

maleic anhydride-derived compatibilizers. Regarding the use of MLO (**Figure 5e**), the surface morphology is similar to that observed with ELO. It seems that particles are fully embedded in the PBS matrix. Regarding DDSA, a small gap between the ASF particles and the surrounding matrix can be observed (**Figure 5f**). This gap is still higher for acrylic-derived compatibilizers (**Figure 5g** and **Figure 5h**), thus corroborating the obtained mechanical properties. In addition to a large gap between the particles, AA leads to more brittle materials.

3.3. Thermal characterization of compatibilized PBS/ASF composites

A comparative plot of the DSC thermograms of neat PBS, uncompatibilized PBS/ASF composite and compatibilized composites can be seen in **Figure 6**. The endothermic peak located between 115 – 125 ºC corresponds to the melt process of the crystalline PBS. The simple addition of 30 wt% ASF leads to a slight decrease of the melt peak temperature of about 1 ºC, while the crystallinity increases. It has been widely reported the nucleant effect that cellulose fillers can provide to semicrystalline polymers. In fact, Frollini *et al.* have reported a clear nucleant effect of several lignocellulose fillers on PBS. They also reported negligible effects of lignocellulosic fillers on main thermal transitions of PBS composites with lignocellulosic fillers [27, 45]. **Table 3** summarizes the main thermal parameters obtained from DSC. Addition of the different compatibilizers gives an additional decrease in the melt peak temperature of about 5 ºC. The most important thing is that the melt process proceeds at relatively low temperatures and this is important when working with lignocellulosic fillers that are quite sensitive to thermal degradation.

Figure 6

Table 3

With regard to thermal degradation at high temperatures (decomposition), thermogravimetric analysis (TGA) shows that ASF exerts important changes in PBS thermal behaviour as it can be concluded by comparing the TGA thermograms in **Figure 7**. Degradation of a lignocellulosic fillers takes place in four different stages: water removal, hemicellulose degradation, cellulose degradation and, finally, lignin degradation. The slight weight loss comprised between 80 – 100 ^{o}C, corresponds to water removal as lignocellulosic fillers (and their composites) have great tendency to absorb moisture [46]. At higher temperatures, hemicellulose degradation occurs, which is followed by cellulose degradation. Both degradation processes involve complex reactions (dehydration, decarboxylation, among others) as well as breakage of C-H, C-O and C-C bonds. Lignin is more thermal stable and undergoes degradation in a broad temperature range from 250 ^{o}C up to 450 ^{o}C due to aromatic rings. Lignin degradation generates water, methanol, carbon monoxide and carbon dioxide [44]. These findings have also been reported by Perinovíc *et al.* corroborating the superior thermal stability of lignin compared to hemicellulose and cellulose [47]. The changes in the thermal behaviour of PBS are related to addition of ASF. Lee *et al.* have reported a change in the degradation mechanism in other polymeric composite materials with lignocellulosic reinforcements. This is because the degradation of the material begins at the surface of the fillers [48], thus preventing the matrix to degrade. Cellulose (main component of ASF) degradation overlaps with the PBS degradation and can contribute to delay PBS degradation as degradation starts on cellulosic particles [49, 50].

Figure 7

Uncompatibilized PBS/ASF composite is thermally stable up to 330 ºC thus indicating that conventional processing conditions are far from the onset degradation temperature. Addition of different compatibilizer agents leads to different effects on thermal stability. PBS is a highly thermally stable polyester. It is more stable even than PLA as reported by Hassan *et al.* [51]. As it can be seen in **Figure 7a**, the onset degradation temperature of all compatibilized PBS/ASF composites is lower, due to the plasticization effect that all compatibilizers provide to composites. In fact, the onset degradation temperature ($T_{5\%}$ stands for the temperature at which, a weight loss of 5% occurs) of uncompatibilized PBS/ASF composite changes from 335.9 ºC down to values of 295 ºC for all the vegetable oil-based compatibilizers and even, to lower values of 270 ºC for composites compatibilized with DDSA and AA. **Figure 7b** shows a comparative plot of the first derivative (DTG) curves for PBS/ASF composites with different compatibilizers. It can be clearly seen that uncompatibilized PBS/ASF shows the maximum thermal stability while addition of whatever compatibilizer leads to a previous degradation peak which could be related to excess compatibilizer. The degradation temperature peak (T_{max}), corresponding to the maximum degradation rate and can be clearly identified in the corresponding DTG graphs. It can be seen that the temperature peaks move to lower temperatures by 5 – 15 ºC, depending on the compatibilizer.

3.4. Thermomechanical properties of compatibilized PBS/ASF composites

Figure 8a shows the evolution of storage modulus (G') of PBS/ASF composites with different compatibilizers. As temperature increases, the characteristic G' values decrease due to a softening effect. The results in **Figure 8** are in total accordance with

previous mechanical results. In fact, the lowest G' values are obtained for the MLO-compatibilized PBS/ASF composite as observed in tensile properties. In general, all the G' curves are located below the one of the uncompatibilized PBS/ASF composite, thus indicating lower rigidity, excepting for the curve corresponding to the composite compatibilized with AA which shows the highest G' values of the herein developed materials. The fact that G' curves are below of that of the uncompatibilized composites indicates that all compatibilizers contribute to increase mechanical ductile properties (in more or less extent). **Figure 8b** shows the evolution of the damping factor (tan δ). The α-relaxation peak located between -21 ^{o}C and -31 ^{o}C corresponds to the glass transition temperature (T_g) of PBS. The T_g is located between -26 ^{o}C to -29 ^{o}C for composites compatibilized with modified-vegetable oils (ELO, ESBO, MLO). DDSA leads to a T_g of -23 ^{o}C while acrylic compatibilizers lead to a T_g value of -31 ^{o}C. It should be noted that the reduction in T_g is relatively low. Consequently, the plasticizing effect is not extremely high. The decrease in T_g may be due to the flexibility provided by triglyceride molecules that interact with PBS chains and cellulose particles. In fact, in some systems a slight increase in T_g is observed [52].

Figure 8

In addition to the dynamic mechanical analysis, dimensional stability has been assessed by thermomechanical analysis (TMA). Specifically, the coefficient of linear thermal expansion (CLTE) above the T_g, is summarized in **Table 5**. As expected, PBS is a flexible polymer and its corresponding composite with 30 wt% ASF shows a moderate CLTE of 128.1 μm m^{-1} ^{o}C^{-1}. All compatibilizers provide a plasticization effect as observed previously with other mechanical properties. Regarding the epoxy-based

compatibilizers, ELO seems to be more effective as leads to a CLTE of 143.3 μm m^{-1} $^{o}C^{-1}$, slightly higher than that of the uncompatibilized composite. ESBO-compatibilized composite shows a CLTE of almost 170 μm m^{-1} $^{o}C^{-1}$, which is noticeably higher than ELO-compatibilized composite.

Table 5

This could be directly related to the number of epoxy groups per triglyceride. ELO, with an average of 6 oxirane rings/triglyceride can establish more interactions with both PBS and ASF, while ESBO, with about 4 epoxy groups per molecule, leads to more flexible materials. It is worthy to note the interesting results obtained with MLO as compatibilizer, in terms of dimensional stability as its corresponding CLTE is 134.3 μm m^{-1} $^{o}C^{-1}$ which is similar to that of the uncompatibilized composite.

4. Conclusions

Wood plastic composites with a poly(butylene succinate) (PBS) matrix and 30 wt% almond shell flour (ASF) were successfully manufactured by extrusion and injection moulding. The polymer-particle interactions in the uncompatibilized PBS/ASF composite are very poor, thus leading to a remarkable decrease in both tensile strength and elongation at break. This research work has proved the high effectiveness of some vegetable oil-derived compatibilizers to give high environmentally friendly composites. Specifically, epoxidized linseed oil (ELO) and epoxidized soybean oil (ESBO), both commercially available, gave good compatibilizing effects on PBS/ASF composites by increasing ductile properties such as elongation at break and impact-absorbed energy. In addition to this family of compatibilizers (with the epoxy functionality), maleinized linseed oil (MLO) represents

another alternative to compatibilize biopolyester/lignocellulosic composites without compromising the environmental efficiency. In fact, the best balanced properties are obtained with maleinized linseed oil (MLO). As a general conclusion, it is worthy to note that PBS/ASF composites are very interesting composites for industrial applications which include, automotive parts, construction and building components, furniture, packaging, and so on. In addition, presence of an industrial low cost waste (ASF) contributes to lowering the overall costs of using PBS.

Acknowledgements

This work was supported by the Ministry of Economy and Competitiveness (MINECO) grant numbers MAT2014-59242-C2-1-R and MAT2017-84909-C2-2-R. L. Quiles-Carrillo acknowledges Generalitat Valenciana (GV) for financial support through a FPI grant (ACIF/2016/182) and the Spanish Ministry of Education, Culture, and Sports (MECD) for his FPU grant (FPU15/03812).

References

[1] Pivsa-Art W, Chaiyasat A, Pivsa-Art S, Yamane H, Ohara H. Preparation of Polymer Blends Between Poly(lactic acid) and Poly(butylene adipate-co-terephthalate) and Biodegradable Polymers as Compatibilizers. In: Yupapin P, PivsaArt S, Ohgaki H, editors. 10th Eco-Energy and Materials Science and Engineering Symposium. Amsterdam: Elsevier Science Bv; 2013. p. 549-54.
[2] Garcia-Garcia D, Ferri JM, Montanes N, Lopez-Martinez J, Balart R. Plasticization effects of epoxidized vegetable oils on mechanical properties of poly(3-hydroxybutyrate). Polymer International. 2016;65(10):1157-64.
[3] Dahy H. Biocomposite materials based on annual natural fibres and biopolymers - Design, fabrication and customized applications in architecture. Constr Build Mater. 2017;147:212-20.
[4] Sinha AK, Narang HK, Bhattacharya S. Mechanical properties of natural fibre polymer composites. Journal of Polymer Engineering. 2017;37(9):879-95.
[5] Delgado-Aguilar M, Julian F, Tarres Q, Mendez JA, Mutje P, Espinach FX. Bio composite from bleached pine fibers reinforced polylactic acid as a replacement of glass fiber reinforced polypropylene, macro and micro-mechanics of the Young's modulus. Compos Pt B-Eng. 2017;125:203-10.
[6] Vaisanen T, Haapala A, Lappalainen R, Tomppo L. Utilization of agricultural and forest industry waste and residues in natural fiber-polymer composites: A review. Waste Manage. 2016;54:62-73.
[7] Essabir H, Boujmal R, Bensalah MO, Rodrigue D, Bouhfid R, Qaiss AE. Mechanical and thermal properties of hybrid composites: Oil-palm fiber/clay reinforced high density polyethylene. Mechanics of Materials. 2016;98:36-43.
[8] Lee JM, Ishak ZAM, Taib RM, Law TT, Thirmizir MZA. Mechanical, Thermal and Water Absorption Properties of Kenaf-Fiber-Based Polypropylene and Poly(Butylene Succinate) Composites. J Polym Environ. 2013;21(1):293-302.
[9] Quiles-Carrillo L, Montanes N, Sammon C, Balart R, Torres-Giner S. Compatibilization of highly sustainable polylactide/almond shell flour composites by reactive extrusion with maleinized linseed oil. Industrial Crops and Products. 2018;111:878-88.
[10] Laaziz SA, Raji M, Hilali E, Essabir H, Rodrigue D, Bouhfid R, et al. Bio-composites based on polylactic acid and argan nut shell: Production and properties. International Journal of Biological Macromolecules. 2017;104:30-42.
[11] Essabir H, Achaby MEI, Hilali EIM, Bouhfid R, Qaiss A. Morphological, Structural, Thermal and Tensile Properties of High Density Polyethylene Composites Reinforced with Treated Argan Nut Shell Particles. J Bionic Eng. 2015;12(1):129-41.
[12] Valdes A, Fenollar O, Beltran A, Balart R, Fortunati E, Kenny JM, et al. Characterization and enzymatic degradation study of poly(epsilon-caprolactone)-based biocomposites from almond agricultural by-products. Polym Degrad Stabil. 2016;132:181-90.
[13] Essabir H, Bensalah MO, Rodrigue D, Bouhfid R, Qaiss A. Structural, mechanical and thermal properties of bio-based hybrid composites from waste coir residues: Fibers and shell particles. Mechanics of Materials. 2016;93:134-44.
[14] Garcia-Garcia D, Carbonell A, Samper MD, Garcia-Sanoguera D, Balart R. Green composites based on polypropylene matrix and hydrophobized spend coffee ground (SCG) powder. Compos Pt B-Eng. 2015;78:256-65.
[15] Valdes A, Vidal L, Beltran A, Canals A, Garrigos MC. Microwave-Assisted Extraction of Phenolic Compounds from Almond Skin Byproducts (Prunus amygdalus): A Multivariate Analysis Approach. J Agric Food Chem. 2015;63(22):5395-402.
[16] Zahedi M, Khanjanzadeh H, Pirayesh H, Saadatnia MA. Utilization of natural montmorillonite modified with dimethyl, dehydrogenated tallow quaternary ammonium salt

as reinforcement in almond shell flour-polypropylene bio-nanocomposites. Compos Pt B-Eng. 2015;71:143-51.
[17] Kim SJ, Moon JB, Kim GH, Ha CS. Mechanical properties of polypropylene/natural fiber composites: Comparison of wood fiber and cotton fiber. Polymer Testing. 2008;27(7):801-6.
[18] Labidi S, Alqahtani N, Alejji M. Effect of Compatibilizer on Mechanical and Physical Properties of Green Composites Based on High Density Polyethylene and Date Palm Fiber2013.
[19] Kim HS, Yang HS, Kim HJ. Biodegradability and mechanical properties of agro-flour–filled polybutylene succinate biocomposites. Journal of Applied Polymer Science. 2005;97(4):1513-21.
[20] Tecchio P, Freni P, De Benedetti B, Fenouillot F. Ex-ante Life Cycle Assessment approach developed for a case study on bio-based polybutylene succinate. Journal of Cleaner Production. 2016;112:316-25.
[21] Mizuno S, Maeda T, Kanemura C, Hotta A. Biodegradability, reprocessability, and mechanical properties of polybutylene succinate (PBS) photografted by hydrophilic or hydrophobic membranes. Polym Degrad Stabil. 2015;117:58-65.
[22] Vytejckova S, Vapenka L, Hradecky J, Dobias J, Hajslova J, Loriot C, et al. Testing of polybutylene succinate based films for poultry meat packaging. Polymer Testing. 2017;60:357-64.
[23] Calabia BP, Ninomiya F, Yagi H, Oishi A, Taguchi K, Kunioka M, et al. Biodegradable Poly(butylene succinate) Composites Reinforced by Cotton Fiber with Silane Coupling Agent. Polymers. 2013;5(1):128-41.
[24] Phiriyawirut M, Mekaroonluck J, Hauyam T, Kittilaksanon A. Biomass-Based Foam from Crosslinked Tapioca Starch/Polybutylene Succinate Blend. J Renew Mater. 2016;4(3):185-9.
[25] Liu LF, Yu JY, Cheng LD, Qu WW. Mechanical properties of poly(butylene succinate) (PBS) biocomposites reinforced with surface modified jute fibre. Composites Part a-Applied Science and Manufacturing. 2009;40(5):669-74.
[26] Terzopoulou ZN, Papageorgiou GZ, Papadopoulou E, Athanassiadou E, Reinders M, Bikiaris DN. Development and Study of Fully Biodegradable Composite Materials Based on Poly(butylene succinate) and Hemp Fibers or Hemp Shives. Polym Compos. 2016;37(2):407-21.
[27] Frollini E, Bartolucci N, Sisti L, Celli A. Biocomposites based on poly(butylene succinate) and curaua: Mechanical and morphological properties. Polymer Testing. 2015;45:168-73.
[28] Tserki V, Matzinos P, Panayiotou C. Novel biodegradable composites based on treated lignocellulosic waste flour as filler. Part II. Development of biodegradable composites using treated and compatibilized waste flour. Composites Part A: Applied Science and Manufacturing. 2006;37(9):1231-8.
[29] Ferri JM, Garcia-Garcia D, Sanchez-Nacher L, Fenollar O, Balart R. The effect of maleinized linseed oil (MLO) on mechanical performance of poly(lactic acid)-thermoplastic starch (PLA-TPS) blends. Carbohydrate Polymers. 2016;147:60-8.
[30] Garcia-Garcia D, Fenollar O, Fombuena V, Lopez-Martinez J, Balart R. Improvement of Mechanical Ductile Properties of Poly(3-hydroxybutyrate) by Using Vegetable Oil Derivatives. Macromolecular Materials and Engineering. 2017;302(2).
[31] Orellana JL, Mauhar M, Kitchens CL. Cellulose Nanocrystals versus Polyethylene Glycol as Toughening Agents for Poly(Lactic Acid)-Poly(Acrylic Acid) Graft Copolymer. J Renew Mater. 2016;4(5):340-50.
[32] Shibata M, Oyamada S, Kobayashi Si, Yaginuma D. Mechanical properties and biodegradability of green composites based on biodegradable polyesters and lyocell fabric. Journal of Applied Polymer Science. 2004;92(6):3857-63.
[33] Ren M, Song J, Song C, Zhang H, Sun X, Chen Q, et al. Crystallization kinetics and morphology of poly (butylene succinate-co-adipate). Journal of Polymer Science Part B: Polymer Physics. 2005;43(22):3231-41.

[34] Liu L, Yu J, Cheng L, Qu W. Mechanical properties of poly (butylene succinate)(PBS) biocomposites reinforced with surface modified jute fibre. Composites Part A: Applied Science and Manufacturing. 2009;40(5):669-74.
[35] Zhao YQ, Qu JP, Feng YH, Wu ZH, Chen FQ, Tang HL. Mechanical and thermal properties of epoxidized soybean oil plasticized polybutylene succinate blends. Polymers for Advanced Technologies. 2012;23(3):632-8.
[36] Samper MD, Petrucci R, Sanchez-Nacher L, Balart R, Kenny JM. New environmentally friendly composite laminates with epoxidized linseed oil (ELO) and slate fiber fabrics. Compos Pt B-Eng. 2015;71:203-9.
[37] Quiles-Carrillo L, Duart S, Montanes N, Torres-Giner S, Balart R. Enhancement of the mechanical and thermal properties of injection-molded polylactide parts by the addition of acrylated epoxidized soybean oil. Materials & Design. 2018;140:54-63.
[38] Quiles-Carrillo L, Blanes-Martínez M, Montanes N, Fenollar O, Torres-Giner S, Balart R. Reactive toughening of injection-molded polylactide pieces using maleinized hemp seed oil. European Polymer Journal. 2018;98:402-10.
[39] Chaiwutthinan P, Leejarkpai T, Kashima DP, Chuayjuljit S. Poly (lactic acid)/poly (butylene succinate) blends filled with epoxy functionalised polymeric chain extender. Advanced Materials Research: Trans Tech Publ; 2013. p. 644-8.
[40] Torres-Giner S, Montanes N, Boronat T, Quiles-Carrillo L, Balart R. Melt grafting of sepiolite nanoclay onto poly (3-hydroxybutyrate-co-4-hydroxybutyrate) by reactive extrusion with multi-functional epoxy-based styrene-acrylic oligomer. European Polymer Journal. 2016;84:693-707.
[41] Zhang HL, Liang HY, Bian JJ, Hao YP, Han LJ, Wang XM, et al. Influence of acrylic impact modifier on plasticized polylactide blown films. Polymer International. 2014;63(6):1076-84.
[42] Ferri JM, Garcia-Garcia D, Montanes N, Fenollar O, Balart R. The effect of maleinized linseed oil as biobased plasticizer in poly (lactic acid)-based formulations. Polymer International. 2017;66(6):882-91.
[43] Ferri J, Garcia-Garcia D, Sánchez-Nacher L, Fenollar O, Balart R. The effect of maleinized linseed oil (MLO) on mechanical performance of poly (lactic acid)-thermoplastic starch (PLA-TPS) blends. Carbohydrate polymers. 2016;147:60-8.
[44] Frollini E, Bartolucci N, Sisti L, Celli A. Poly (butylene succinate) reinforced with different lignocellulosic fibers. Industrial crops and products. 2013;45:160-9.
[45] Frollini E, Bartolucci N, Sisti L, Celli A. Poly(butylene succinate) reinforced with different lignocellulosic fibers. Ind Crop Prod. 2013;45:160-9.
[46] Faulstich de Paiva JM, Frollini E. Unmodified and modified surface sisal fibers as reinforcement of phenolic and lignophenolic matrices composites: thermal analyses of fibers and composites. Macromolecular Materials and Engineering. 2006;291(4):405-17.
[47] Perinovic S, Andricic B, Erceg M. Thermal properties of poly(L-lactide)/olive stone flour composites. Thermochimica Acta. 2010;510(1-2):97-102.
[48] Lee AT, Kang Y-J, Chang K. Transport properties of carbon nanotubes: Effects of vacancy clusters and disorder. The Journal of Physical Chemistry C. 2011;116(1):1179-84.
[49] Sánchez-Jiménez PE, Pérez-Maqueda LA, Perejón A, Pascual-Cosp J, Benítez-Guerrero M, Criado JM. An improved model for the kinetic description of the thermal degradation of cellulose. Cellulose. 2011;18(6):1487-98.
[50] Sánchez-Jiménez PE, Pérez-Maqueda LA, Perejón A, Criado JM. Generalized master plots as a straightforward approach for determining the kinetic model: the case of cellulose pyrolysis. Thermochimica acta. 2013;552:54-9.
[51] Hassan E, Wei Y, Juiao H, Muhuo Y. Dynamic Mechanical Properties and Thermal Stability of Poly(lactic acid) and Poly(butylene succinate) Blends Composites. J Fib Bioeng Inform. 2013;6(1):85-94.

[52] Martin O, Averous L. Poly (lactic acid): plasticization and properties of biodegradable multiphase systems. Polymer. 2001;42(14):6209-19.

Figure captions

Figure 1. Schematic representation of polycondensation of succinic acid and 1,4-butanediol to give poly(butylene succinate) (PBS).

Figure 2. Schematic representation of the chemical structure of the base polymer and compatibilizers.

Figure 3. Typical stress-strain curves of PBS and uncompatibilized and compatibilized PBS/ASF composites.

Figure 4. Schematic representation of the reactions of epoxy and maleic anhydride groups in PBS/ASF composites.

Figure 5. Scanning electron microscopy (SEM) images corresponding to cryo-fractured surfaces of PBS/ASF composites with different compatibilizers, taken at 1000x a)PBS, b) uncompatibilized, c) ELO-compatibilized, d) ESBO-compatibilized, e) MLO-compatibilized, f) DDSA-compatibilized, g) MMA-compatibilized and h) AA-compatibilized.

Figure 6. Comparative plot of the DSC curves of PBS and PBS/ASF composites with different compatibilizers.

Figure 7. a) Thermogravimetric (TGA) thermograms corresponding to PBS/ASF composites with different compatibilizers and b) first derivative (DTG) curves.

Figure 8. Dynamic mechanical thermal analysis (DMTA) curves of PBS/ASF composites with different compatibilizers, a) storage modulus (G′) and **b)** damping factor (tan δ).

Tables

Table 1. Code and composition of poly(butylene succinate) (PBS)/almond shell flour (ASF) composites with different compatibilizers.

Code	PBS (wt%)	ASF (wt%)	ELO (wt%)	ESBO (wt%)	MLO (wt%)	DDSA (wt%)	MMA (wt%)	AA (wt%)
PBS	100	-	-	-	-	-	-	-
PBS+ASF	70	30	-	-	-	-	-	-
PBS+ASF+ELO	65.5	30	4.5	-	-	-	-	-
PBS+ASF+ESBO	65.5	30	-	4.5	-	-	-	-
PBS+ASF+MLO	65.5	30	-	-	4.5	-	-	-
PBS+ASF+DDSA	65.5	30	-	-	-	4.5	-	-
PBS+ASF+MMA	65.5	30	-	-	-	-	4.5	-
PBS+ASF+AA	65.5	30	-	-	-	-	-	4.5

Table 2. Summary of the mechanical properties of PBS/ASF composites with different functionalities, obtained by tensile, Shore D and Charpy impact tests.

Code	$E_{tensile}$ (MPa)	σ_b (MPa)	Elongation (%)	Shore D hardness	Impact strength (kJ m^{-2})
PBS	417.4 ± 21.1	31.5 ± 0.9	215.6 ± 16,5	60.1 ± 0.5	16.5 ± 0.8
PBS+ASF	787.9 ± 55.8	14.8 ± 0.5	6.3 ± 0.9	71.2 ± 0.3	1.8 ± 0.3
PBS+ASF+ELO	702.2 ± 45.6	13.3 ± 0.4	14.5 ± 1.1	69.0 ± 0.4	3.6 ± 0.4
PBS+ASF+ESBO	715.5 ± 48.9	13.6 ± 0.5	13.1 ± 0.9	68.5 ± 0.4	3.4 ± 0.2
PBS+ASF+MLO	534.6 ± 51.3	13.8 ± 0.3	25.9 ± 1.0	67.2 ± 0.2	3.8 ± 0.5
PBS+ASF+DDSA	718.6 ± 52.5	14.7 ± 0.4	16.9 ± 1.1	69.5 ± 0.5	0.7 ± 0.1
PBS+ASF+MMA	764.8 ± 36.9	15.2 ± 0.6	8.0 ± 0.9	70.5 ± 0.6	3.2 ± 0.2
PBS+ASF+AA	680.2 ± 44.8	13.8 ± 0.4	6.0 ± 0.8	71.9 ± 0.4	0.4 ± 0.1

Table 3. Main thermal properties of PBS and PBS/ASF composites with different compatibilizers obtained by differential canning calorimetry (DSC).

Code	Melt enthalpy ($J\ g^{-1}$)	Melt peak temperature, T_m (°C)	Xc (%)
PBS	65.14 ± 1.96	119.56 ± 1.51	57.65 ± 1.75
PBS+ASF	55.82 ± 1.36	117.96 ± 2.36	70.57 ± 2.12
PBS+ASF+ELO	49.53 ± 1.84	117.46 ± 1.89	67.43 ± 1.87
PBS+ASF+ESBO	52.47 ± 1.15	116.44 ± 1.91	71.43 ± 1.47
PBS+ASF+MLO	52.65 ± 1.72	115.18 ± 1.74	71.68 ± 1.56
PBS+ASF+DDSA	50.63 ± 1.26	114.69 ± 2.08	68.93 ± 2.04
PBS+ASF+MMA	53.16 ± 1.67	115.22 ± 1.53	72.37 ± 1.64
PBS+ASF+AA	47.98 ± 1.96	116.96 ± 0.96	65.32 ± 1.47

Table 4. Summary of the main thermal parameters of the degradation process of PBS/ASF composites with different compatibilizers.

Code	$T_{5\%}$ (°C)	T_{max} (°C)	Residual weight (%)
PBS	338.14 ± 1.43	414.74 ± 1.49	0.39 ± 0.14
PBS+ASF	335.89 ± 1.96	411.90 ± 1.74	1.13 ± 0.09
PBS+ASF+ELO	291.93 ± 1.32	407.64 ± 1.25	0.24 ± 0.12
PBS+ASF+ESBO	295.96 ± 1.08	407.13 ± 1.82	0.43 ± 0.23
PBS+ASF+MLO	295.84 ± 1.22	407.63 ± 1.26	0.68 ± 0.15
PBS+ASF+DDSA	270.63 ± 1.14	406.76 ± 1.08	0.12 ± 0.11
PBS+ASF+MMA	291.33 ± 1.54	403.25 ± 1.66	1.05 ± 0.07
PBS+ASF+AA	268.12 ± 1.58	405.63 ± 1.26	0.64 0.09

Table 5. Variation of the coefficient of linear thermal expansion (CLTE) of PBS/ASF composites with different compatibilizers obtained by thermomechanical analysis (TMA).

Code	CLTE above T_g ($\mu m\ m^{-1}\ ^oC^{-1}$)
PBS+ASF	128.1
PBS+ASF+ELO	143.3
PBS+ASF+ESBO	167.9
PBS+ASF+MLO	134.3
PBS+ASF+DDSA	167.4
PBS+ASF+MMA	167.1
PBS+ASF+AA	184.1

Figure 1

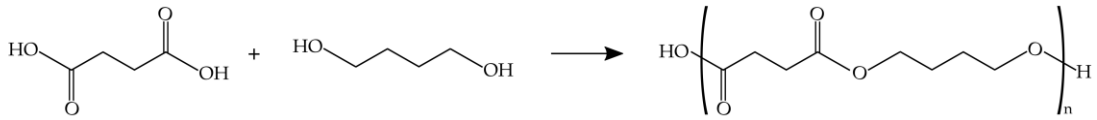

succinic acid 1,4-butanodiol poly(butylene succinate) (PBS)

Figure 2

a) EPOXY FUNCTIONALITY

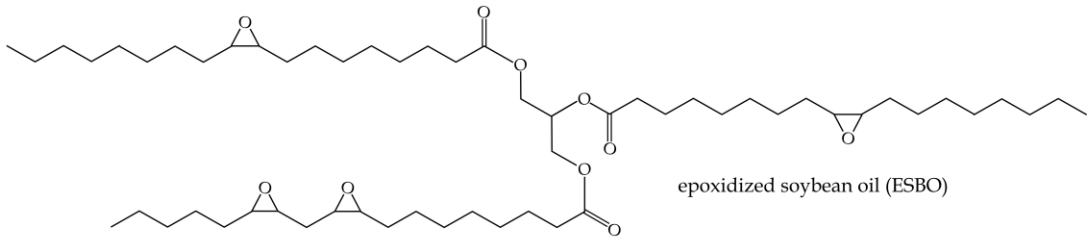

epoxidized soybean oil (ESBO)

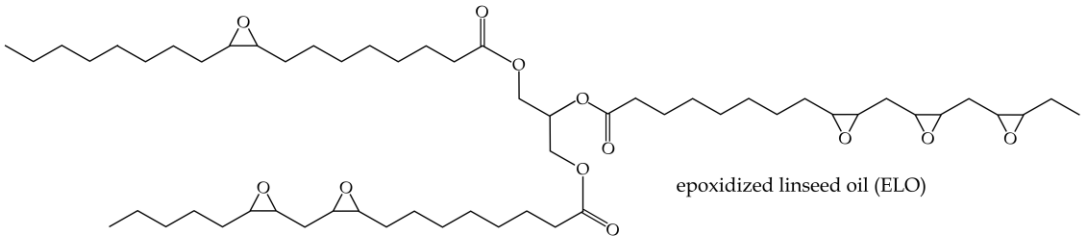

epoxidized linseed oil (ELO)

b) MALEIC ANHYDRIDE FUNCTIONALITY

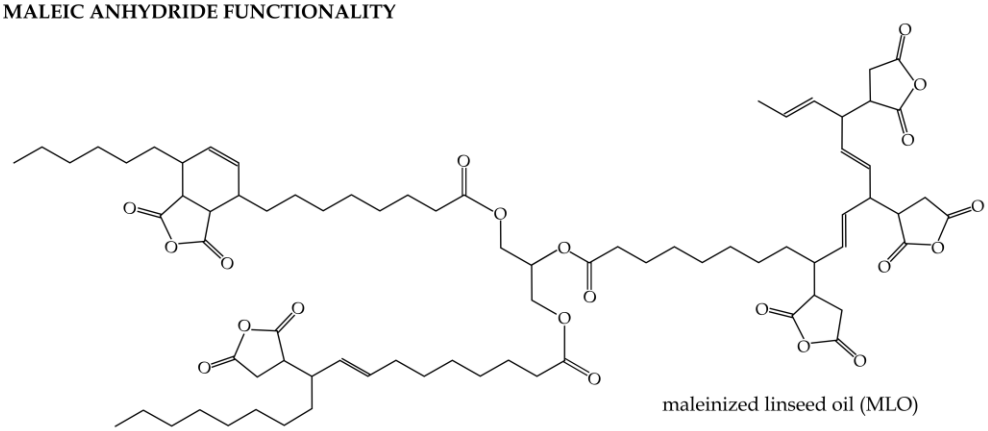

maleinized linseed oil (MLO)

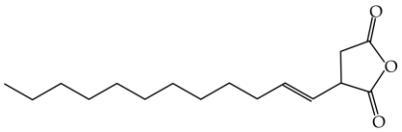

dodecenyl succinic anhydride (DDSA)

c) ACRYLIC FUNCTIONALITY

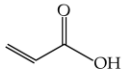

acrylic acid (AA)

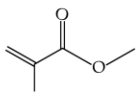

methyl methacrylate (MMA)

Figure 3

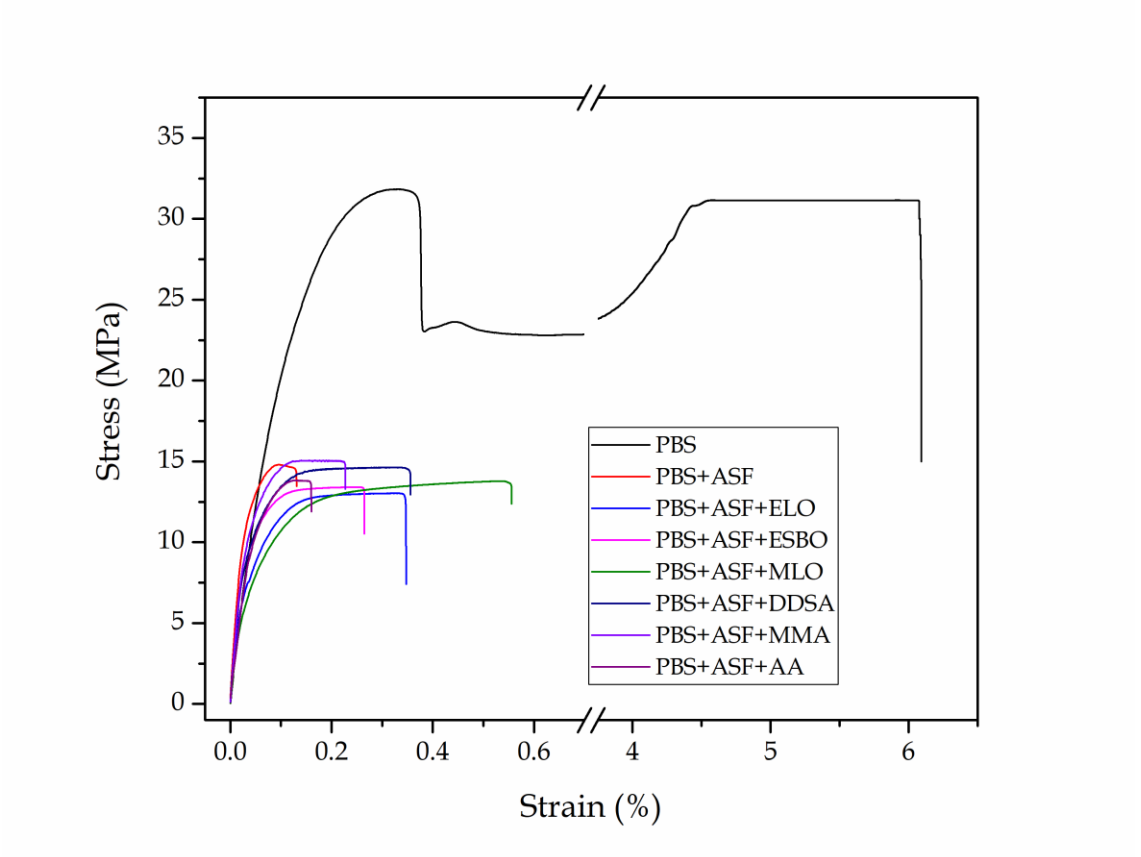
Stress (MPa)
Strain (%)
0
5
10
15
20
25
30
35
0.0
0.2
0.4
0.6
4
5
6
PBS
PBS+ASF
PBS+ASF+ELO
PBS+ASF+ESBO
PBS+ASF+MLO
PBS+ASF+DDSA
PBS+ASF+MMA
PBS+ASF+AA

Figure 4

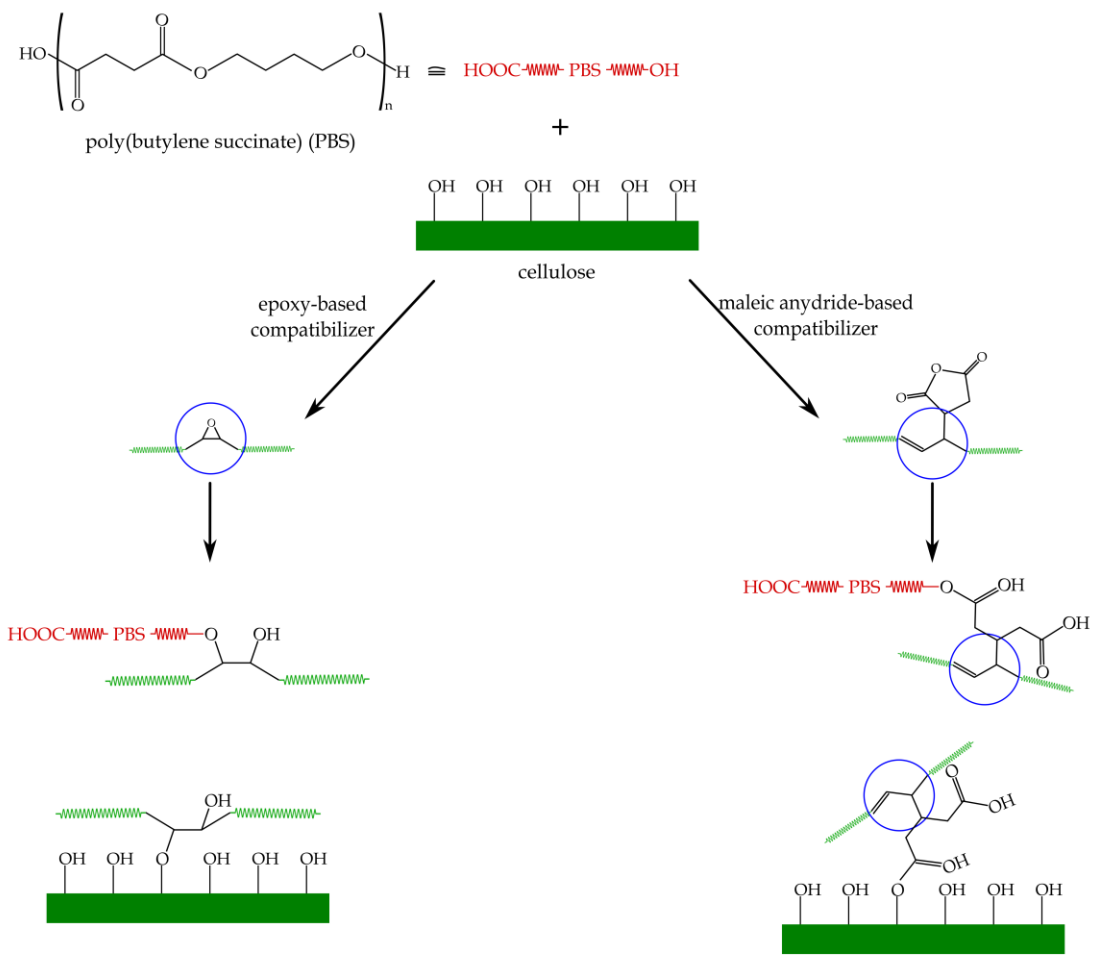
HO
O
O
O
O
H
n
HOOC PBS OH
poly(butylene succinate) (PBS)
+
OH OH OH OH OH OH
cellulose
epoxy-based
compatibilizer
maleic anydride-based
compatibilizer
HOOC PBS O OH
HOOC PBS O OH
OH
OH OH O OH OH OH
O
OH
OH
OH OH O OH OH OH

Figure 5

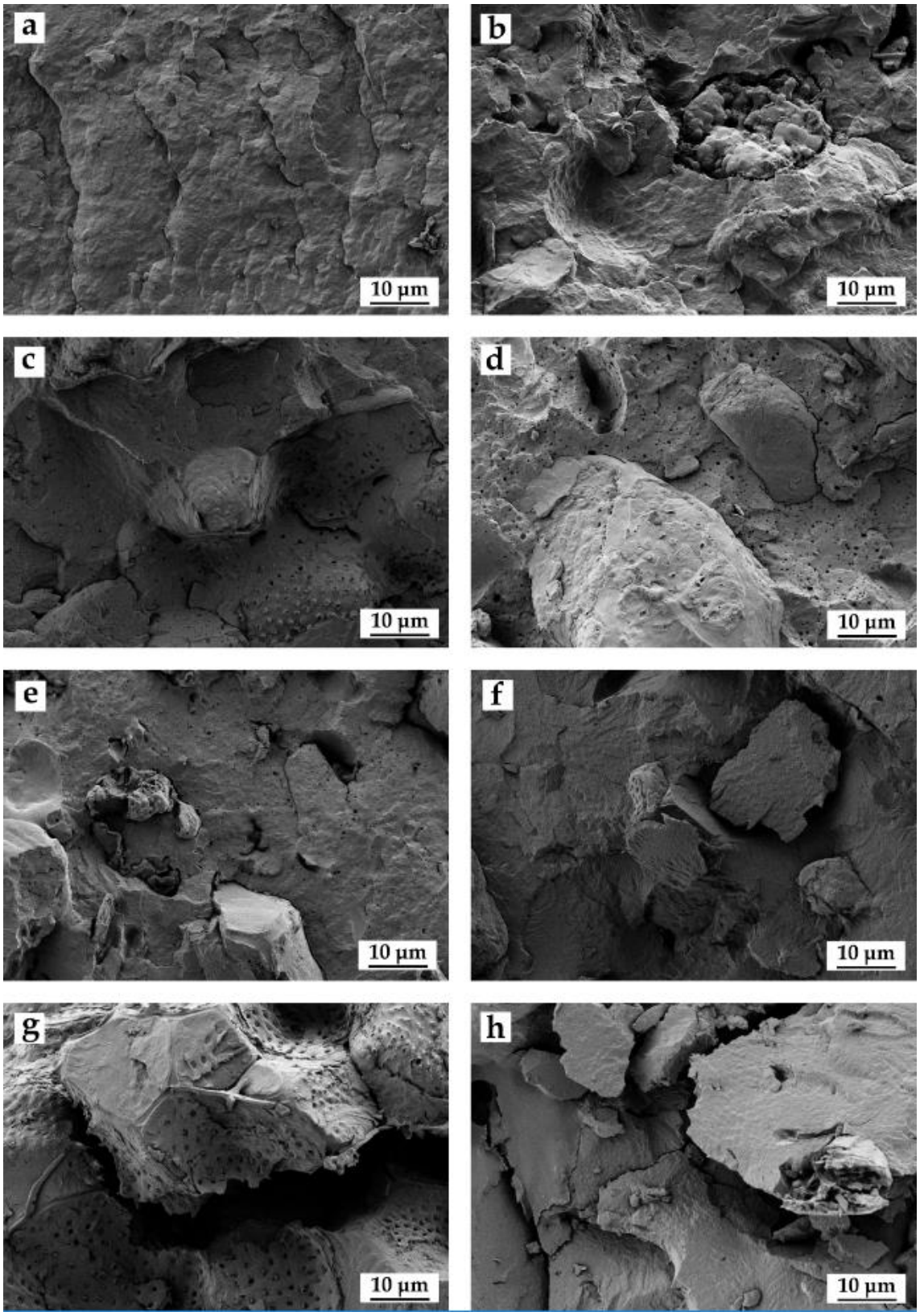

Figure 6

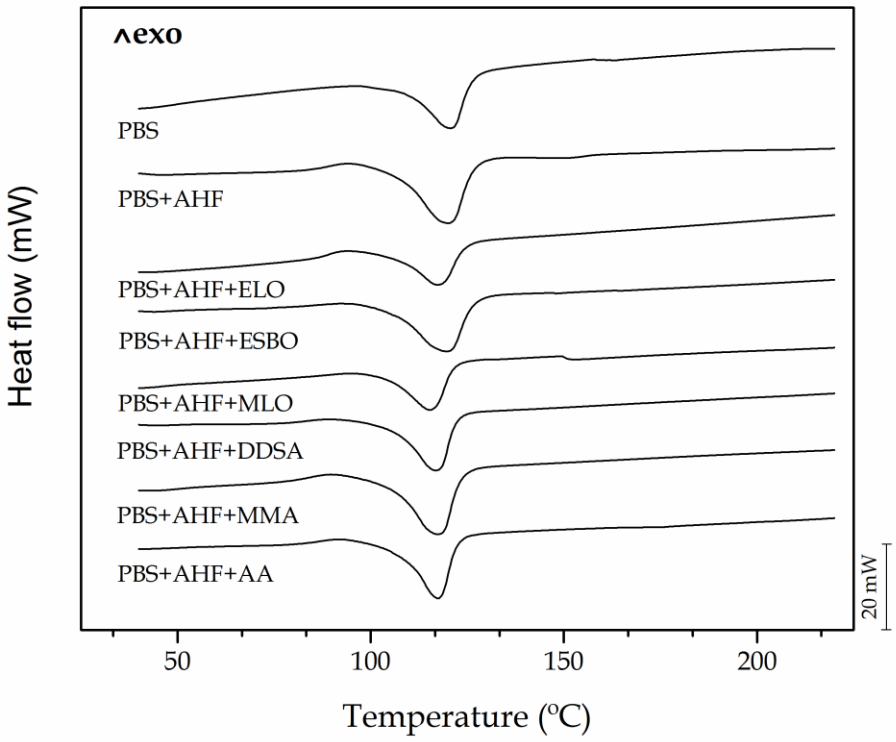
^exo
PBS
PBS+AHF
PBS+AHF+ELO
PBS+AHF+ESBO
PBS+AHF+MLO
PBS+AHF+DDSA
PBS+AHF+MMA
PBS+AHF+AA
20 mW
Heat flow (mW)
50
100
150
200
Temperature (°C)

Figure 7

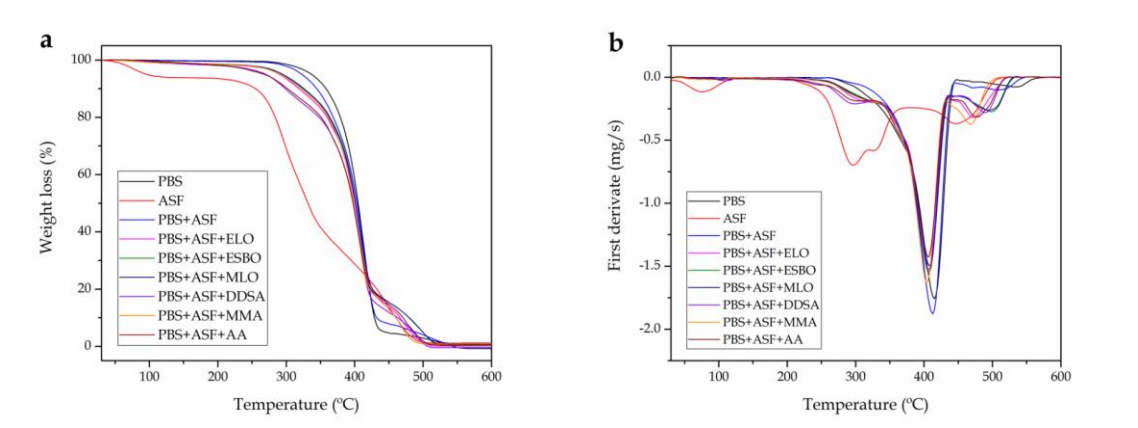

Figure 8